Non-equilibrium capillary pressure of a miscible meniscus

Journal:	*Langmuir*
Manuscript ID	la-2020-036337.R3
Manuscript Type:	Article
Date Submitted by the Author:	n/a
Complete List of Authors:	Vorobev, Anatoliy; University of Southampton, Faculty of Engineering and the Environment ; Tomsk Polytechnic University Prokopev, Sergei; FSBSI Institute of Continuous Media Mechanics of the Ural Branch of Russian Academy of Science Lyubimova, Tatyana; FSBSI Institute of Continuous Media Mechanics of the Ural Branch of Russian Academy of Science; Perm State University

Non-equilibrium capillary pressure of a miscible meniscus

Anatoliy Vorobev,*,†,‡ Sergei Prokopev,¶ and Tatyana Lyubimova¶,§

†*Faculty of Engineering and the Environment, University of Southampton, SO17 1BJ, UK*

‡*Tomsk Polytechnic University, 634050, Russia*

¶*Institute of Continuous Media Mechanics, UB RAS, Perm, 614013, Russia*

§*Perm State University, Perm, 614990, Russia*

E-mail: A.Vorobev@soton.ac.uk

Abstract

We examine the dynamics of a miscible displacement in a capillary, calculating the non-equilibrium capillary pressure of a moving (and slowly-diffusing) miscible meniscus. During the displacement, the capillary pressure varies with time following stretching and smearing of a miscible interface. The capillary pressure remains different from zero for a long time (on a diffusion time scale), slowing down the displacement. This capillary pressure is however completely ignored by all theories currently available for practical modelling of miscible displacements in capillaries and porous matrices.

Introduction

Many engineering processes such as vegetable oil extraction,[1] enhanced oil recovery,[2] CO_2 sequestration,[3] and aquifer and soil remediation[4] are the variations of a solvent-based (or miscible) displacement of a solute liquid from a porous medium. Despite many similarities,

each of these processes is characterised by its own complexity, so that semi-empirical approaches developed e.g. for description of miscible oil recovery do not translate to aquifer remediation, etc. A more universal and detailed understanding of miscible two-phase flows in porous media can be achieved through the pore-level analysis[5] that represents a porous matrix by a network of interconnected capillaries, reducing the initial study to modelling of a flow in a single capillary (an element of a porous matrix), which is undertaken in the present work.

It is well known that the liquid/liquid displacement is controlled by capillary forces. When capillary forces dominate, the meniscus has an axisymmetric shape, moving with the same speed as the rest of the liquids and pushing the displaced liquid like a piston. At stronger injection rates (or for a mixture of two liquids with a lower surface tension coefficient), the meniscus in a capillary becomes stretched by the flow, adopting a finger-type shape. In the limiting case (when the longitudinal size of a meniscus exceeds the capillary's length), the injected liquid just penetrates through the middle section of a capillary, leaving nearly half of the displaced liquid on the capillary's wall.

A contact between two miscible liquids can also result in a prolonged equilibration dynamics with clearly visible phases separated by interfaces, whose evolution can be explained only by surface tension forces.[6–9] The dynamic (non-equilibrium) surface tension associated with miscible interfaces is in particular evidenced by observations of near-spherical shapes of rising/descending inclusions in a miscible environment,[6] gravity-capillary waves on a miscible interface,[10] Faraday and frozen waves on miscible interfaces subjected to vibrations,[11] etc. Still, surface tension coefficients of miscible boundaries are usually small, so this effect is rarely taken into account in practical models. The dynamics of two-phase miscible flows in confined geometries, e.g. in pores of a porous matrix, can however be strongly influenced by the non-equilibrium surface tension, which motivates improved understanding and modelling of this effect.

Experimental observations of a miscible displacement in capillaries are reported in the

work.[12] The observations are available for relatively short time durations, with a clear meniscus observed during the entire displacement run. These experiments permitted estimation of the surface tension coefficient for a miscible water-glycerol/water mixture, $\sigma_* \sim 4.3 \cdot 10^{-4}\,\mathrm{N{\cdot}m^{-1}}$. The capillary pressure in the capillaries that were used in the experiment[12] (with diameters $> 1\,\mathrm{mm}$) was too little, which explains the relatively good agreement of the experimental data with the modelling results that are derived on the basis of the model that neglects the surface tension forces.[13] For capillaries characterised by smaller diameters (more relevant for porous media), the capillary effects associated with miscible interfaces will be significant. Indeed, in a capillary with the diameter $d_* = 10^{-4}\,\mathrm{m}$, the capillary pressure can be estimated as $p_{c*} \sim \sigma_*/d_* \sim 1\,\mathrm{Pa}$. The imposed pressure gradient in a porous matrix depends on application, but, e.g. for oil recovery or for CO_2 sequestration, the imposed pressure gradient can be estimated as $\Delta p_*/L_* \sim (10^7\mathrm{Pa})/(10^3\mathrm{m}) = 10^4\,\mathrm{Pa{\cdot}m^{-1}}$, and hence the imposed pressure difference on the scale of a single pore is $(\Delta p_*)_1 \sim (\Delta p_*/L_*)d_* \sim 1\,\mathrm{Pa}$, the same order as the capillary pressure of a miscible meniscus.

It should be also mentioned that there are other measurements of the non-equilibrium surface tension coefficients for the same glycerol/water mixture, which report different, conflicting values of the surface tension coefficient. Namely, the later paper[14] by the same research group concludes that the effective surface tension coefficient for this mixture should be lower than $2 \cdot 10^{-4}\,\mathrm{N{\cdot}m^{-1}}$, the paper[15] confirms that the value reported in the work[12] is probably an over-estimation, and, finally, the recent measurement[16] produces a much lower value $2.5 \cdot 10^{-7}\mathrm{N{\cdot}m^{-1}}$.

We would like to emphasise that the authors of the experiment[12] clearly observe the difference between their results and those that would be obtained for two liquids separated by a boundary with no surface tension. The reported surface tension coefficient is the numerical measure of the difference. One however may argue that the authors[12] do not take into account all factors that may affect the results, and that they relate the difference to a single effect, the effective interfacial stress of a miscible interface. One could add that, though a single value

of the effective surface tension coefficient is reported, the non-equilibrium capillary forces acting between miscible boundaries are process- (time-) dependent, gradually diminishing in strength upon progression of the dissolution process,[6,17] which could also explain the differences in the results cited above.

All the above-cited values of the surface tension coefficient are obtained via the comparisons of a miscible system and an immiscible system, neglecting the mixing dynamics. Thus, all the reported values can simply correspond to the different stages of mixing, which should be characterised by different values of the non-equilibrium surface tension. For instance, the paper[16] reports the measurements of the non-equilibrium surface tension obtained by using the spinning droplet tensiometry technique. The molecular-level mixing in a spinning capillary can occur faster as compared with the displacement-like experiments.[12,15] Indeed, in a rapidly spinning capillary, the mixing is enhanced by barodiffusion and convective motion, which intensities are proportional to the square of the angular velocity of the tube's rotations (and dominance of centrigual effect over gravity is a principal idea of the spinning drop tensiometry).[18] In particular, convective vortices are evidenced by the umbrella-like shapes of the droplet's ends that are observed at long time scales.[8]

In our current work, we do not aim to find the correct value of the effective surface tension coefficients. For our work, it is important that the existence of non-equilibrium surface tension is experimentally confirmed by different researchers. We extend this observation by noting that the displacement in capillary tubes should be controlled by the non-equilibrium capillary pressure. We aim to investigate the role/strength of capillary forces associated with miscible interfaces, as well the variation of capillary forces with time. We would like to note that the standard Darcy-based approaches developed for practical description of two-phase flows in porous media are currently incapable of capturing similar properties of the capillary forces.[19–21]

Physical model

We apply the phase-field approach that we use as a consistent physics-based macroscopic description of the dynamics of slowly miscible liquids. This model in particular is able to describe the non-equilibrium surface tension properties of miscible interfaces.[22–24]

The evolution of a binary mixture is set by the following governing equations,

$$\frac{\partial \vec{u}}{\partial t} + (\vec{u} \cdot \nabla)\vec{u} = -\nabla \frac{\Pi}{\rho} + \frac{\eta}{\rho}\nabla^2 \vec{u} - C\nabla\mu, \tag{1}$$

$$\frac{\partial C}{\partial t} + (\vec{u} \cdot \nabla)C = \frac{\alpha}{\rho}\nabla^2 \mu, \tag{2}$$

$$\nabla \cdot \vec{u} = 0. \tag{3}$$

Here, $\vec{u}$ is the fluid velocity that is defined as the mass average velocity of a two-phase fluid particle, Π is the modified pressure that is determined by using an incompressibility constraint, and C is the concentration defined as the mass fraction of one of the liquids in a mixture. In this study we neglect the effects of gravity. We assume that the evolution of a binary mixture remains isothermal (latent heat of the phase transition is neglected). We also assume that the difference in the viscosities of two liquids (the dependence of the viscosity coefficient on concentration) can be neglected, so only one coefficient of viscosity, η, is introduced.

By inspection of the above equations, one can notice that the Navier-Stokes equation (1) includes an additional force that is called the Korteweg force and that determines the morphology of a liquid/liquid boundary. In addition, in the phase-field approach, the diffusion flux is set to be proportional to the gradient of the chemical potential.

The equation that defines the chemical potential reads

$$\mu = \frac{df_0}{dC} - \epsilon\nabla^2 C. \tag{4}$$

This expression includes the classical and non-classical parts. The classical part is defined by the specific free energy function, f_0, that sets the thermodynamic behaviour of a mixture. The choice of the free energy function determines the equilibrium states of a binary mixture. One of the options (that is adopted in this work) is the Landau free energy,[25]

$$f_0 = a(C - C_{cr})^2 + b(C - C_{cr})^4, \tag{5}$$

which presumes that the evolution of a binary mixture with an upper critical (consolute) point is studied. Two phenomenological parameters, a and b, determine the particular choice of a mixture. It could be shown that near the critical point, a can be either negative or positive, while b is just positive.

The magnitude of the non-classical (capillary) term in expression (4) is set by the capillary constant ϵ.

The intensity of the diffusion process is determined by the mobility coefficient α, which value can be correlated with the classical diffusion coefficient by the relation, $D = \frac{\alpha}{\rho}\frac{d\mu}{dC}$.

The governing equations are to be supplemented by the boundary conditions: the no-slip boundary condition ($\vec{u} = 0$) for the velocity field, the absence of the diffusion flux through the wall ($\partial\mu/(\partial n) = 0$) for the chemical potential, and a condition for the concentration field that defines the wetting properties.

The governing equations (1)-(4) are solved in the non-dimensional form. For that, we accept the following scales for length, time, velocity, pressure, and chemical potential,

$$d_*,\ \frac{d_*}{V_*},\ V_*,\ \rho V_*^2,\ \mu_*. \tag{6}$$

Here d_* is the typical length scale (the capillary's diameter, or the size of a pore), and V_* and μ_* are the typical values of velocity and chemical potential. For the velocity scale, it is

convenient to accept the maximum of the Poisseuille flow in a capillary,

$$V_* = \frac{\Delta p_*}{L_*}\frac{d_*^2}{8\eta}. \tag{7}$$

Here L_* is the capillary's length. The scale of chemical potential, μ_*, is given by the value of the phenomenological parameter, b, so that $\mu_* = b$. In addition we also shift the reference point for the concentration, $C \to (C - C_{cr})$.

The dimensionless form of the governing equations (1)-(4) reads,

$$\frac{\partial \vec{u}}{\partial t} + (\vec{u}\cdot\nabla)\vec{u} = -\nabla\Pi + \frac{1}{Re}\nabla^2\vec{u} - \frac{1}{M}C\nabla\mu, \tag{8}$$

$$\frac{\partial C}{\partial t} + (\vec{u}\cdot\nabla)C = \frac{1}{Pe}\nabla^2\mu, \tag{9}$$

$$\nabla\cdot\vec{u} = 0. \tag{10}$$

$$\mu = 2AC + 4C^3 - Cn\nabla^2 C. \tag{11}$$

Equations (8)-(11) include the following non-dimensional parameters,

$$Re = \frac{\rho V_* d_*}{\eta}, \quad Pe = \frac{\rho V_* d_*}{\alpha\mu_*}, \quad M = \frac{V_*^2}{\mu_*}, \quad Cn = \frac{\epsilon}{\mu_* d_*^2}. \tag{12}$$

These are the Reynolds, Peclet, Mach and Cahn numbers. The Reynolds number number determines the importance of the viscous force. The Peclet number determines the relative importance of the hydrodynamic and diffusive effects. The Peclet number also determines the slippage rate of a contact line.[24,26] The Mach number (that should not be confused with the classical Mach number, although it also determines the relative importance of the thermodynamic and hydrodynamic effects) determines the strength of the Korteweg force, and hence determines the strength of the surface tension forces. The Cahn number is proportional to the capillary constant, and hence it also controls the strength of the surface tension forces.

There is one additional non-dimensional parameter that defines the thermodynamic behaviour of a mixture,

$$A = \frac{a}{\mu_*}. \tag{13}$$

This parameter plays the role of the 'temperature' of a mixture (the difference in the

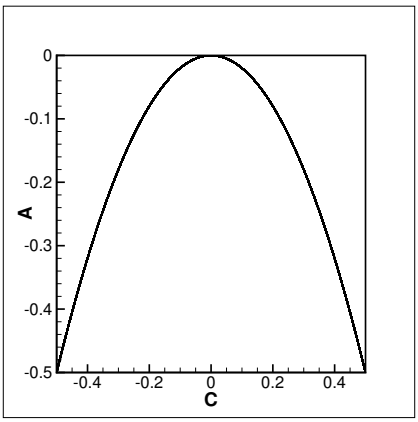

Figure 1: Phase diagram for a binary mixture with an upper critical (consolute) point with the coordinates (0,0).

mixture temperature from its critical point). Indeed, figure 1 depicts the shape of the phase-diagram defined by the Landau function (5). One may see that $A = 0$ corresponds to the critical (consolute) point, if $A > 0$ the mixture is always homogeneous in equilibrium, and if $A < 0$ then the mixture can be heterogeneous in equilibrium, with two equilibrium levels of concentrations, $C = \pm\sqrt{-A/2}$. When $A = -1/2$, the equilibrium levels of concentrations are $\pm 1/2$, which correspond to two pure phases. This value of A is deemed to be the minimum possible value.

In addition, we would like to mention that the strength of the capillary effects is traditionally determined by the surface tension coefficient. Within the phase-field approach, the surface tension forces are determined by a number of alternative parameters, while the surface tension coefficient can be calculated by using the formula,[22,27]

$$\sigma = \frac{ReCa}{M}\frac{E_i}{S} = \frac{ReCaCn}{M}\frac{1}{S}\int_V (\nabla C)^2 dV. \tag{14}$$

Here, E_i is the interfacial energy that is scaled by $\rho\mu_* d_*^3$, σ is the coefficient of surface tension that is scaled by σ_* (the dimensional value of the surface tension coefficient), and S is the area of the interface scaled by d_*^2.

The equation for the surface tension coefficient (14) introduces an additional non-dimensional parameter, the capillary number,

$$Ca = \frac{\eta V_*}{\sigma_*}. \tag{15}$$

The capillary parameter will only appear in the definition of the surface tension coefficient (14), which makes convenient to plot the results of calculation of the surface tension coefficient by using the ratio σ/Ca.

Problem statement. Numerical approach

In the present work the governing equations (8)-(11) are solved for a capillary that is represented by a plane layer with two plates of length $L = L_*/d_*$ separated by a unit distance. The consideration is restricted to the two-dimensional problem, with the Cartesian coordinates, x and y, along and across the layer. For the initial state we assume that a capillary is occupied with one liquid (with the concentration level $C = 1/2$) that stays at rest ($\vec{u} = 0$), and the injection of the second liquid (with the concentration level $C = -1/2$) starts at $t = 0$ at the left end of a capillary.

The governing equations are supplemented by the following boundary conditions: at the upper and lower plates,

$$y = 0, 1: \quad u_x = u_y = 0,\ \frac{\partial \mu}{\partial y} = 0,\ \frac{\partial C}{\partial y} = 0; \tag{16}$$

at the left end of a capillary,

$$x = 0: \quad p = p_1,\ \frac{\partial \mu}{\partial x} = 0,\ \frac{\partial C}{\partial x} = 0; \tag{17}$$

and at the right end,

$$x = L: \quad p = p_2,\ \frac{\partial \mu}{\partial x} = 0,\ \frac{\partial C}{\partial x} = 0. \tag{18}$$

For the wetting boundary condition (imposed by the condition on the field of concentration), we use $\partial C/(\partial n) = 0$ (here $\vec{n}$ is a normal to the wall), i.e. we assume that the interface remains always orthogonal to the wall. This simplification however does not negate the capillary pressure that is defined by the dynamic contact angle.[24,28]

The reference point for the pressure field is set at the right (outlet) end of a capillary (i.e. $p_2 = 0$). The pressure level at the left (inlet) end of a capillary is always set as

$$p_1 = \frac{8L}{Re}. \tag{19}$$

In a single-phase flow, this pressure difference, $p_1 - p_2$, will generate the Poiseuille's flow with the flow rate $Q_1 = 2/3$. The action of capillary forces will slow down the flow, reducing the flow rate, which is discussed below.

The governing equations are solved numerically using the formulation of the primitive variables, pressure-velocity, and using the fractional-step (or projection) method that is implemented on the basis of the finite difference approach.[29,30] A novel algorithm[21] developed for implementation on graphical processing units is employed. The necessity to trace the interface between two liquids enforces higher requirements on the numerical resolution. We conduct the calculations using a uniform mesh with the size of 1/600 across and along the capillary. In our earlier works,[21,24] we found that this resolution is sufficient for the accurate reproduction of the dynamics of a two-phase fluid mixture in a capillary. The calculations were fulfilled by using the NVidia Tesla V100 graphical cards. A typical time that is needed for calculation of a full displacement run was about 7-10 days.

Values of non-dimensional parameters

We consider a mixture with the typical density $\rho \sim 10^3\,\mathrm{kg{\cdot}m^{-3}}$, the density contrast $\phi \sim 0.1$ and the viscosity coefficient $\eta \sim 10^{-3}\,\mathrm{Pa{\cdot}s}$. The mixture saturates a capillary with the diameter $d_* \sim 10^{-4}\,\mathrm{m}$. The displacement flow is set by the imposed pressure gradient. For the pressure gradient of $\Delta p_*/L_* \sim 10^4\,\mathrm{Pa{\cdot}m^{-1}}$ (that is typical e.g. in geological applications), formula (7) gives an estimate of the velocity as $V_* \sim 10^{-2}\,\mathrm{m{\cdot}s^{-1}}$. The Reynolds number can then be estimated as $Re \sim 1$, which is accepted for our calculations. In addition, let us provide the estimates for the time scale, $d_*/V_* \sim 10^{-2}\,\mathrm{s}$, and the pressure scale, $\rho_* V_*^2 \sim 0.1\,\mathrm{Pa}$.

Next, we discuss the choice of the Peclet number and the capillary's length. In this study we aim to observe the diffusive dynamics. The typical diffusion time that defines smearing of an interface is given by $t_d = d_*^2/D$, and the typical hydrodynamic time that defines the propagation of a meniscus in a capillary is given by $t_h = L_*/V_*$. The ratio of these times is

$$\frac{t_d}{t_h} = \frac{V_* d_*}{D}\frac{d_*}{L_*} = Pe\frac{d_*}{L_*} = \frac{Pe}{L}. \tag{20}$$

The experiment[12] was conducted with a capillary of diameter $d_* \geq 1\mathrm{mm}$ and length $L_* = 1\mathrm{m}$ (the non-dimensional length $L \sim 1000$). The flow was controlled by an externally-set pressure difference, which determined the flow velocity in a capillary and the value of the Peclet number. Hence, in the experiment,[12] the ratio of the diffusive and hydrodynamic times was equal to 1 when $Pe \sim 1000$, which perfectly agrees with the reported findings. Indeed, it is reported that the critical Peclet number, that limited the authors' abilities to conduct optical observations, was exactly 1000: at higher Peclet numbers the miscible interface remained sharp, well visible, during the movement of a meniscus through the full capillary's length; and the meniscus became too smeared (indistinguishable) when Peclet number was less than 1000.

In numerical simulations, owing to computational constraints, it is impossible to choose

the capillary length comparable to the one of the experiment ($L \sim 1000$). The results reported below are given for the capillaries with the length, $L = 40$. According to equation (20), to have the diffusive effects clearly visible in so short capillaries, the Peclet number needs to be taken as low as $Pe \sim 40$. Nevertheless, owing to the amount of data that could be generated by numerical simulations (in other words, owing to sensitivity of a numerical experiment), we start noticing the diffusion-based changes in the flow dynamics even when $Pe = 1000$. Thus, we conduct the simulations with several different Peclet numbers, in the range $Pe = 300 - 1000$, and the results are reported for $Pe = 300$ and $Pe = 1000$.

The value of the Cahn number determines the interface thickness (the thickness of a thermodynamically equilibrium interface is $\sim \sqrt{-Cn/A}$). The real interface thickness is very small, a few molecular layers, which is zero for a macroscopic theory. For the sake of numerical calculations, however, the interface is smeared, represented by a boundary of a finite thickness. To reproduce the physically relevant behaviour, the Cahn number needs to be taken very small, which makes the numerical simulations challenging due to necessity to resolve a small spatial scale. To solve this problem, the numerical simulations for different Cahn numbers are conducted with the aim to reveal the behaviour of a binary mixture when the Cahn number tends to zero (it is sufficient to achieve the limit when the interface thickness becomes much smaller than other spatial scales). A similar study was fulfilled in our earlier works,[21,31] where we found that the Cahn number, $Cn = 10^{-4}$, can be used to generate good (physically-relevant) results. Thus, this value is accepted for the calculations of the current work.

The value of the Mach number can be selected from observations of e.g. the shape of a meniscus that is set by the capillary forces. We will show the results for different Mach numbers, discussing the differences in the shapes and dynamics of menisci.

Finally, since we are primarily interested in modelling of a miscible displacement, we perform the key calculations for the values of parameter A greater than $A = -0.5$. Any value of parameter A that is different from -0.5 makes the two liquids miscible, as this

makes the equilibrium values of concentration different from the initial levels, $C = \pm 1/2$ (see figure 1). However, we also conduct the calculations for $A = -0.5$ to generate the results for immiscible interfaces, for references and for comparisons.

Results

Immiscible displacement

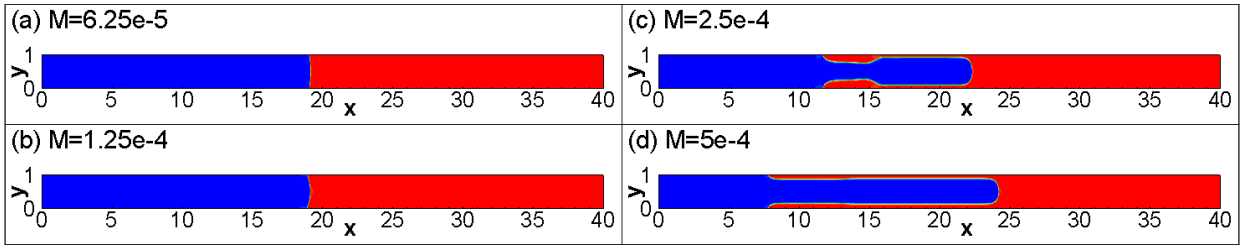

Figure 2: Immiscible displacement. The fields of concentration at $t = 31$ for $Pe = 300$, $Re = 1$, $Cn = 10^{-4}$, $A = -0.5$, and different Mach numbers as indicated in the figures.

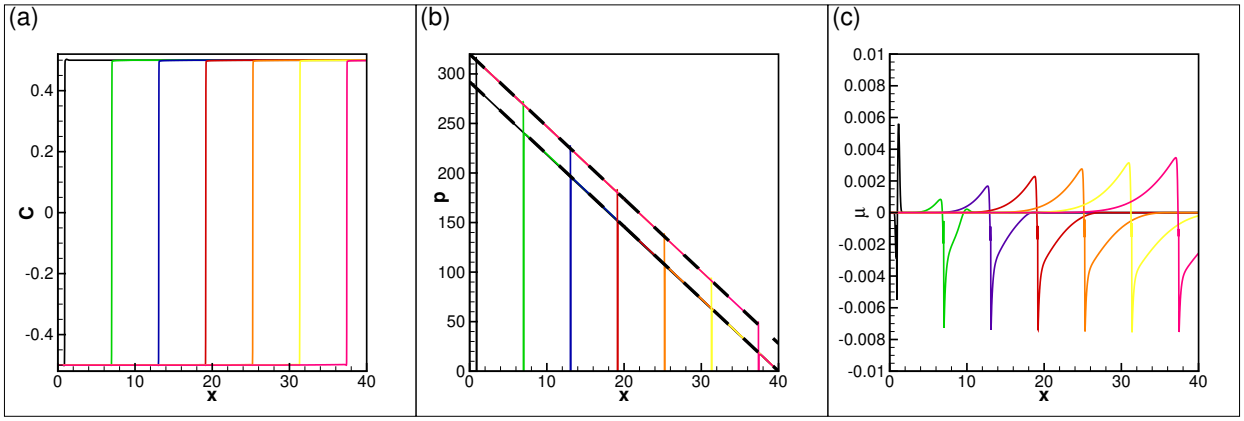

Figure 3: Immiscible displacement. The profiles of concentration (a), pressure (b), and chemical potential (c) along the capillary's centreline for the time moments: 1, 11, 21, 31, 41, 51, and 61. The results are obtained for $A = -0.5$, $Pe = 300$, $Re = 1$, $Cn = 10^{-4}$, and $M = 6.25 \cdot 10^{-5}$. In (b) the thick dashed lines show the pressure distributions in the displacing and displaced liquids, given by $\Delta p - (\Delta p - p_c)x/L$ and $(\Delta p - p_c)(1 - x/L)$, with $p_c = 28$ and $\Delta p = 320$ for the calculation shown.

Figures 2 and 3 show the fields of concentration, pressure and chemical potential for an immiscible displacement. At lower Mach numbers (figures 2a,b), the surface tension effects

are strong, the meniscus is compact, with a piston-like shape, and the meniscus' shape does not change along its propagation in a capillary. At higher Mach numbers (figures 2c,d), the finger-like displacement is observed. Figures 2 also reveal that slippage of a contact line along the capillary's walls occurs slower at higher Mach numbers, which explains why the displacement occurs so differently at different values of the Mach number.

In all cases there is no interfacial diffusion; the concentration levels in both liquids remain unchanged. There are some smaller variations of the chemical potential near the meniscus, with amplitudes below 0.01, which need to be associated with the level of accuracy of an immiscible model. The pressure linearly drops along the capillary with a jump (by the value of the capillary pressure) at the meniscus (see figure 3b). The capillary pressure remains constant during the entire displacement run.

The capillary pressure of a meniscus can be also calculated as the difference between the two-phase flow rate, Q, and the single-phase flow rate, $Q_1 = 2/3$,[21,32]

$$\frac{p_c}{\Delta p} = \left(1 - \frac{Q}{Q_1}\right). \tag{21}$$

Figures 4a,b show that both the flow rates and the capillary pressures for immiscible flows remain constant even for a finger-like displacement. For $M = 6.25 \cdot 10^{-5}$, the capillary pressure in figure 4b is $p_c = 28$, which coincides with the value obtained from the pressure profiles in figure 3b.

The capillary pressure can be also determined from another classical formula that is written here using the above-accepted scales,

$$p_c = \frac{1}{CaRe}\frac{2\sigma\cos\theta}{R}. \tag{22}$$

Here $R = 1/2$ is the capillary's radius. By inserting the capillary pressure obtained with equation (21) into equation (22) one can find the dynamic contact angle for the meniscus. At $M = 6.25 \cdot 10^{-5}$, the so-calculated contact angle is $\theta = 79^0$, which is also in agreement

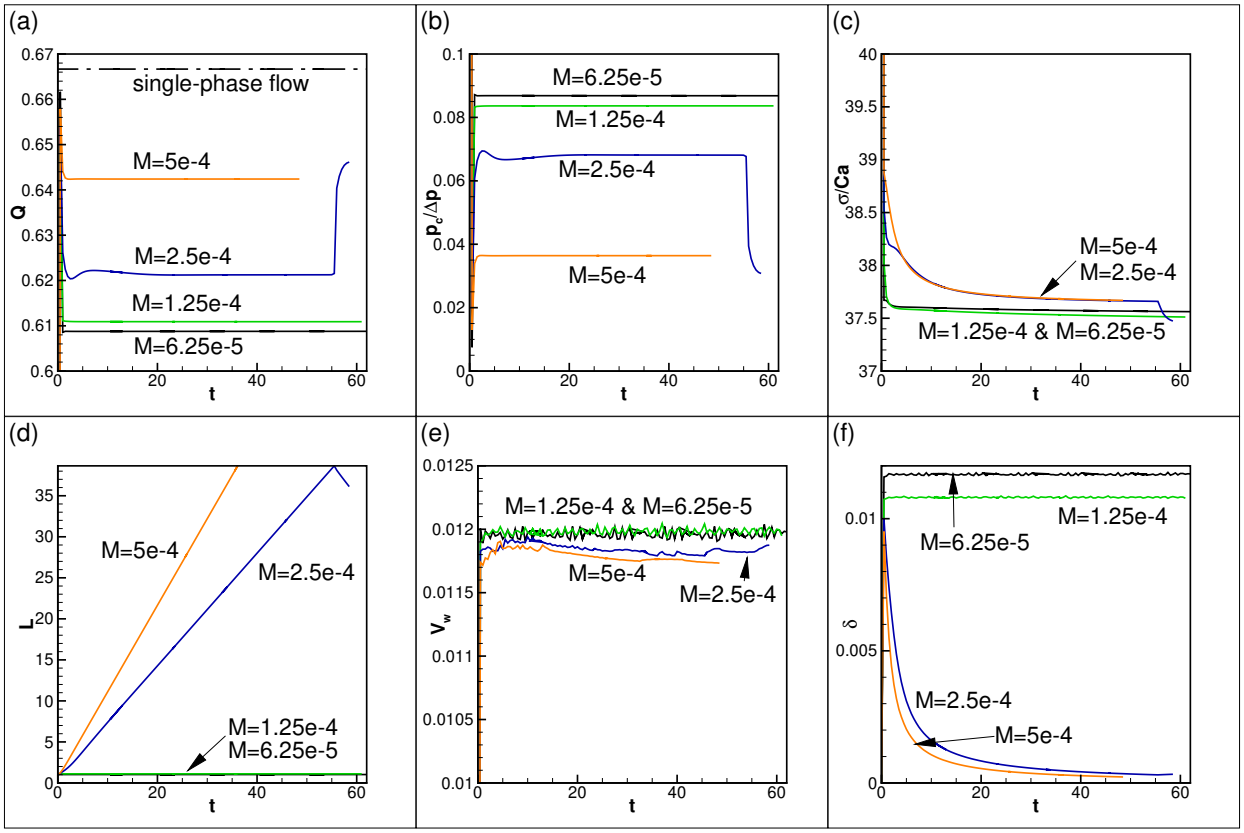

Figure 4: Immiscible displacement. The temporal variations of the flow rate (a), the capillary pressure divided by the imposed pressure difference (b), the surface tension coefficient divided by the capillary number (c), the length of the meniscus (d), the volume of the interfacial zone (e), and the thickness of the interface (f). The the results are obtained for $Pe = 300$, $Re = 1$, $Cn = 10^{-4}$, $M = 6.25 \cdot 10^{-5}$, and $A = -0.5$.

with the shape of the meniscus depicted in figure 2a.

The calculations of the surface tension coefficients shown in figure 4c reveal quite small variations with the change of the Mach number that are insufficient to explain the differences in the capillary pressure. The stronger dependencies on the Mach number should be explained by different rates of slippage of a contact line at different Mach numbers.

Figure 4f indicates that stretching of the meniscus results in its thinning. The similar observations were previously reported for a liquid/liquid interface in a binary mixture that experiences the Rayleigh-Taylor instability.[33] Figure 4e shows that the volume of the meniscus, which is calculated as the volume of the zone for which $|C| \leq 0.2$, remains constant. The changes of this volume should be driven by diffusion, which does not exist in the case of immiscible displacement. The constant value of the meniscus volume gives an easy correlation between the interface length (shown in figure 4d) and interface thickness: $V_w = L\delta$, which helps to understand why the thickness of a stretched interface decreases.

Some further results for immiscible displacements can be also found in our recent publications.[21,24] As noted above, one of the aims to conduct the immiscible calculations in this work is to substantiate the choice of the value of the Mach number. Traditionally, it is expected that the immiscible displacement occurs with the piston-like displacement, and that is why we adopt the value $M = 6.25 \cdot 10^{-5}$ for our further (miscible) calculations.

Miscible displacement

The typical snapshots of miscible displacements are depicted in figure 5. The snapshots are shown for two values of parameter A, taken below and above the consolute point. The fingering displacements are observed in both cases. However, for $A = -0.1$, one can notice that, at the start of the displacement run, the bubble-like shape of the meniscus develops that is replaced by the finger-type shape at the later time moments. These two modes correspond to different levels of interfacial stresses in figure 2. This observation indicates that the effective surface tension coefficient associated with a miscible interface slowly reduces

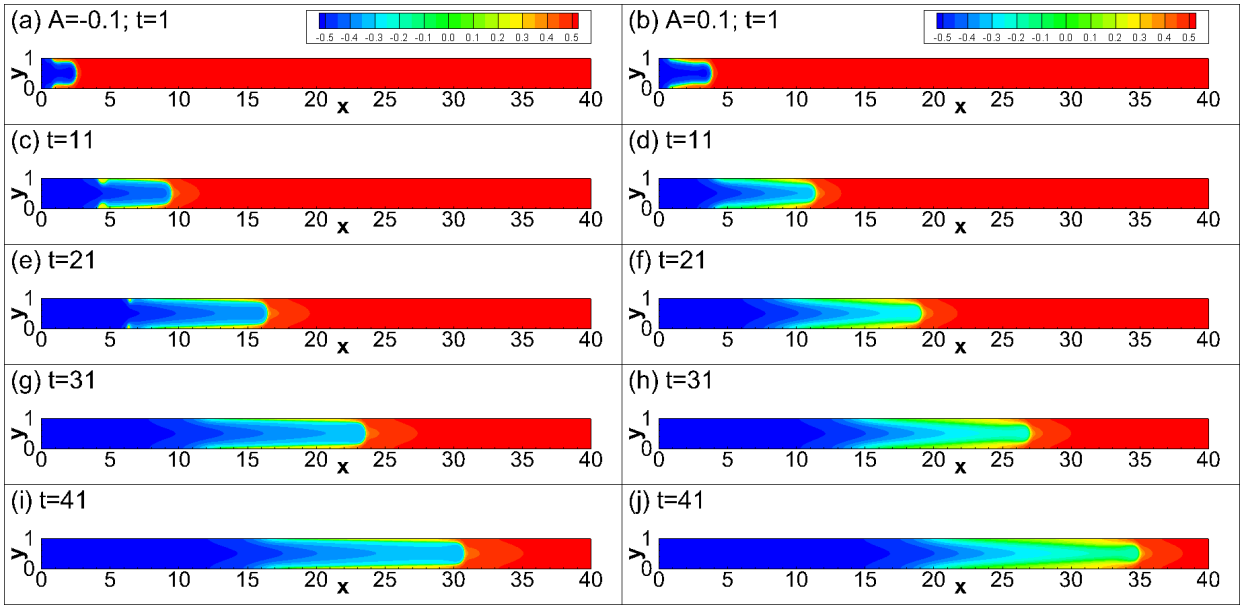

Figure 5: Miscible displacement. The fields of concentration at different time moments, as indicated in the pictures, for $M = 6.25 \cdot 10^{-5}$, $Pe = 300$, $Re = 1$, $Cn = 10^{-4}$, for $A = -0.1$ (a,c,e,g,i) and $A = 0.1$ (b,d,f,h,j).

with time, which is discussed below in details.

Figure 6 depicts the profiles of the concentration (figures 6a,b,c), pressure (figures 6d,e,f), and chemical potential (figures 6g,h,i) along the capillary's centreline for miscible displacements that occur under different mixture temperatures. Figure 7 depicts the temporal variations of the integral characteristics for a miscible displacement: the flow rate (figure 7a), the capillary pressure (figure 7b), the surface tension coefficient (figure 7c), the length of the meniscus (figure 7d), the thickness of the meniscus (figure 7e), and the average concentrations in the displaced and displacing phases (figure 7f).

The interfacial diffusion results in smearing of an interface, with primary diffusion of the displaced liquid into the displacing phase. At lower values of parameter A (lower mixture temperatures), the piston-like displacement can still be observed, with the time-independent flow rate, capillary pressure, and meniscus shape. At higher A, the displacement occurs through development of a finger in the middle of a capillary, and all integral parameters experience complex temporal variations.

It is interesting to note that a (slightly) miscible piston-like displacement may occur with

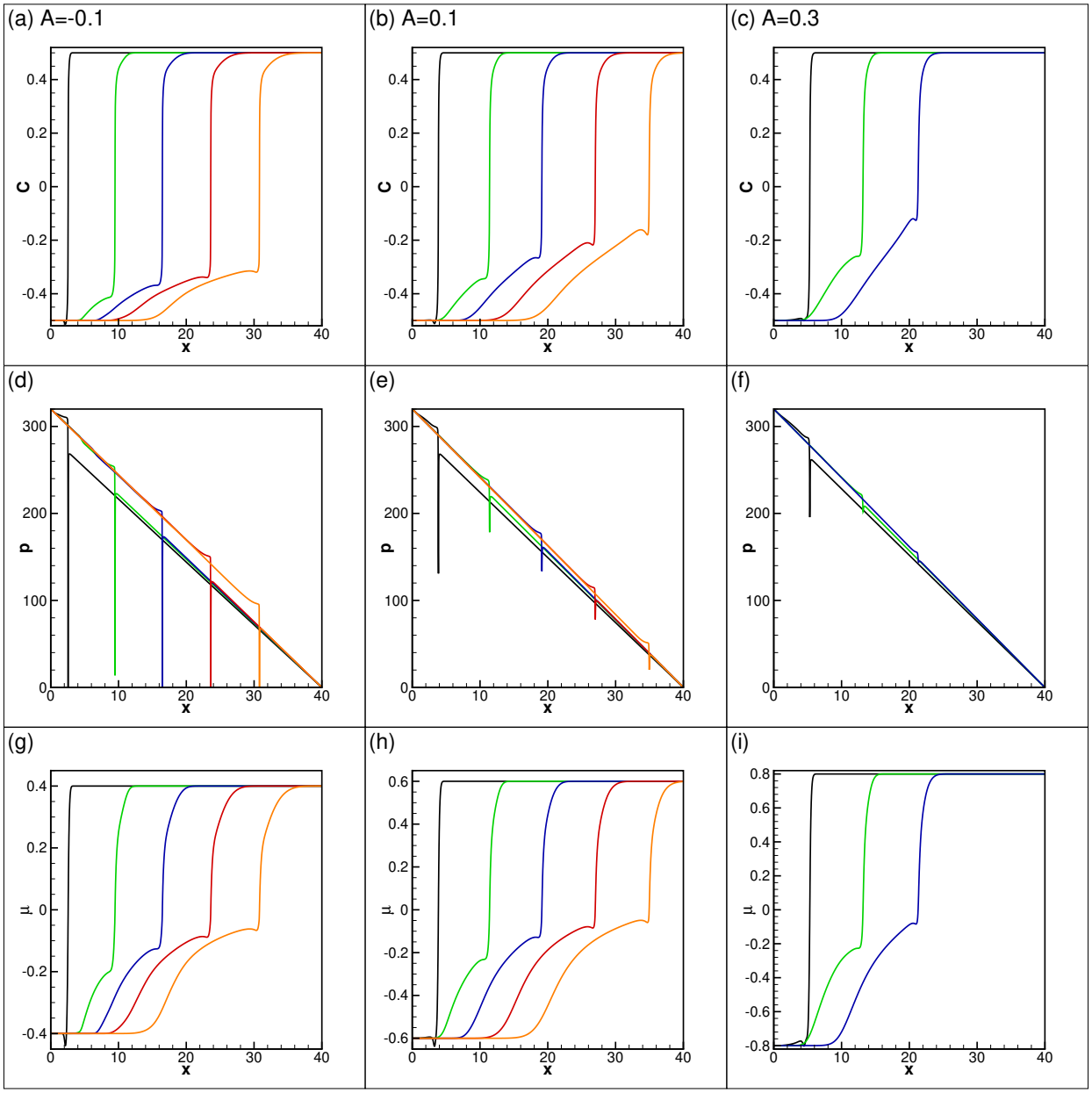

Figure 6: Miscible displacement. The profiles of concentration (a-c), pressure (d-f) and chemical potential (g-i) along the centreline for the different time moments, starting from $t = 1$ with an increment of 10 units in non-dimensional time. The results are obtained for $Pe = 300$, $Re = 1$, $Cn = 10^{-4}$, $M = 6.25 \cdot 10^{-5}$, and three different A, $A = -0.1$ (a,d,g), $A = 0.1$ (b,e,h), and $A = 0.3$ (c,f,i).

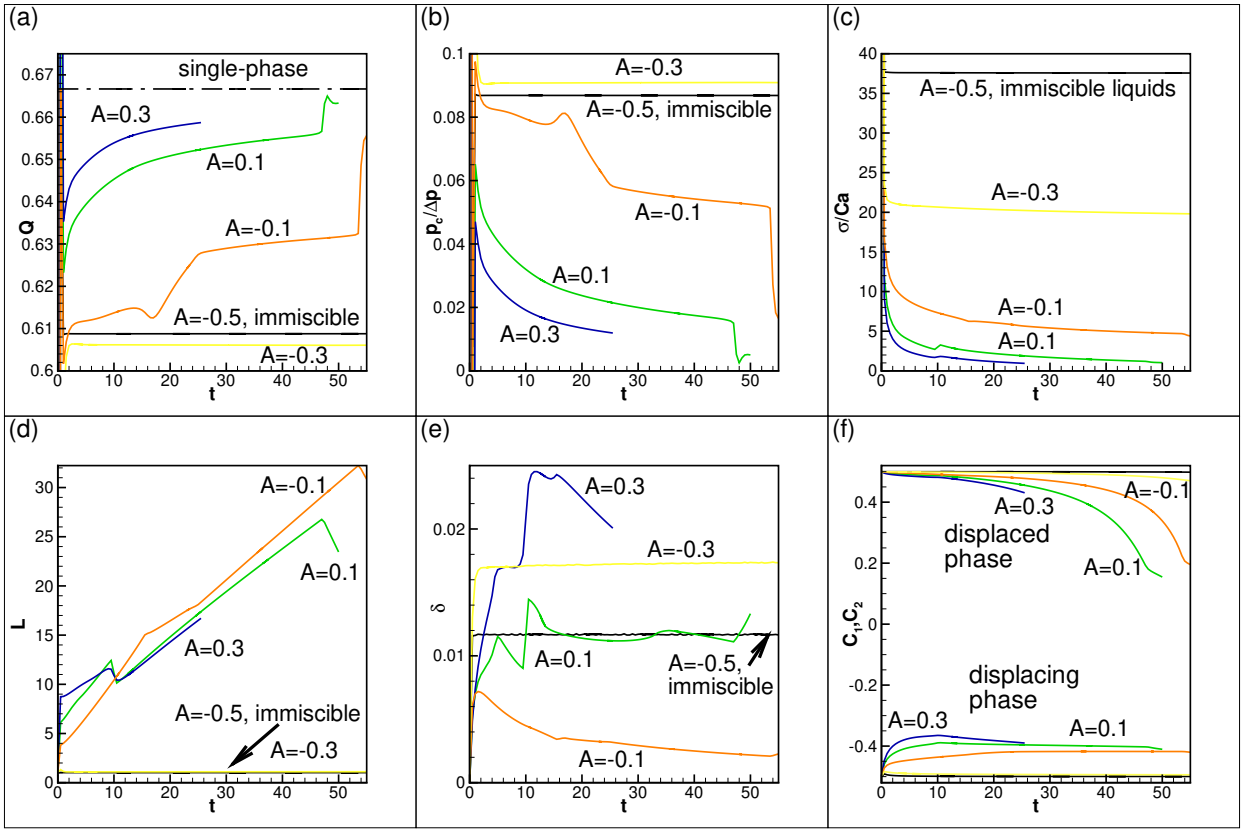

Figure 7: Miscible displacement. (a) The volumetric flow rate vs. time; (b) the ratio between the capillary pressure and applied pressure difference vs. time; (c) the surface tension coefficient vs. time; (d,e) the length and thickness of a meniscus vs. time; and (f) the average concentrations in the displaced and displacing phases. The results are obtained for $Pe = 300$, $Re = 1$, $Cn = 10^{-4}$, $M = 6.25 \cdot 10^{-5}$, and for different A as indicated in the figures.

a slower rate as compared with an immiscible displacement (compare e.g. the displacements at $A = -0.3$ and $A = -0.5$). The surface tension of a miscible interface is always lower (see figure 7c), but the the meniscus has a different shape, a lower dynamic contact angle, and hence the displacement is characterised by the lower capillary pressure.

An evolution of a finger-shaped miscible meniscus also differs from an immiscible case. In particular, stretching of a miscible displacement does not lead to its noticeable thinning (see figure 7e). For a miscible interface, the thickness of an interfacial volume grows with time due to diffusion, so the thickness of an interface rapidly grows at the moment of contact of liquids and remains nearly constant at the later moments.

Figures 6g-i depict the profiles of the chemical potential along the centreline. Comparison of figures 6g-i and figure 3c indicates an increase of the gradient of the chemical potential (hence an intensification of interfacial diffusion) as the value of parameter A grows.

Figure 7f shows the levels of average concentrations in the displaced and displacing phases. For an immiscible displacement, these two levels remain constant, equal to $\pm 1/2$. For a miscible displacement, the diffusion predominantly occurs into the displacing phase. The changes in the averaged concentration of the displaced phase become stronger towards the break-through moment, when the meniscus approaches the outlet end of a capillary and the volume of the displaced phase becomes small.

The key result of our work can be drawn from the shapes of the pressure profiles depicted in figures 6d-f, which show a gradual decrease in the value of the capillary pressure (given by the jump in pressure profile across the meniscus). At sufficiently high values of the parameter A, the capillary pressure may become non-existent at some point, so the flow becomes single-phase. This result is confirmed by the curves in figure 7b.

We also investigated the time variations of the capillary pressure at A taken above the consolute point (see figure 8). For the longer (diffusion-based) variations of the capillary pressure, we found that at $A = 0.1$ the capillary pressure decays as $0.086t^{-0.43}$, at $A = 0.3$ the time dependence is $0.06t^{-0.5}$, and at $A = 0.5$ the time dependence is $0.046t^{-0.53}$. The

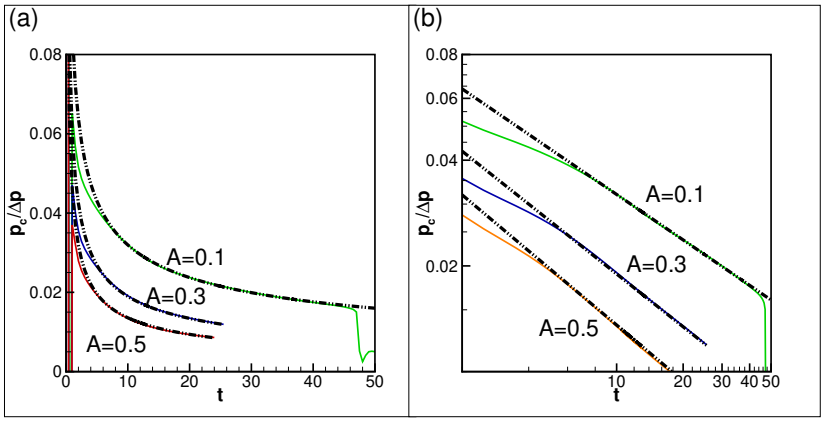

Figure 8: Miscible displacement. The time variations of the capillary pressure in normal (a) and logarithmic (b) scales for three different values of parameter A that are taken above the consolute point. The results are obtained for $Pe = 300$, $Re = 1$, $Cn = 10^{-4}$, $M = 6.25 \cdot 10^{-5}$, and for different A as indicated in the figures. The dashed lines show the following dependencies, $0.086 \cdot t^{-0.43}$, $0.06 \cdot t^{-0.5}$ and $0.046 \cdot t^{-0.53}$.

time-dependence always remains close to $t^{-0.5}$-law, which is typical for a diffusive-driven process. The observed time-law depends on the mixture temperature (the value of A), which should be explained by the effects of hydrodynamics, e.g. by the differences in the lengths of the meniscus that define the contact of the phases.

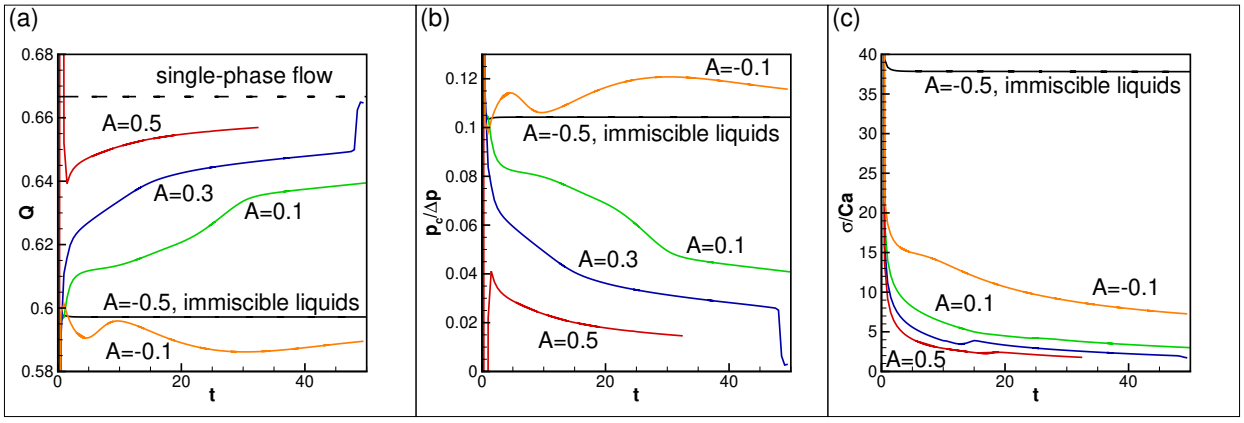

Figure 9: Miscible displacement. (a) The volumetric flow rate vs. time; (b) the capillary pressure divided by the applied pressure difference vs. time; and (c) the surface tension coefficient vs. time. The results are obtained for $Pe = 1000$, $Re = 1$, $Cn = 10^{-4}$, $M = 6.25 \cdot 10^{-5}$, and for different A as indicated in the figures.

Finally, in figure 9 we show that all above observations remain generally valid for all miscible menisci. For instance, at higher Peclet number, the diffusion becomes weaker, but

still, the time-dependent (non-equilibrium) capillary pressure of a miscible meniscus can be clearly determined.

Conclusion

In conclusion, we would like to note that the notion of non-equilibrium surface tension associated with miscible interfaces was cited by Korteweg,[34] and even earlier. Nevertheless, despite a century-long study of the capillary properties of miscible interfaces, measurements of non-equilibrium surface tension still remain a topic of active research, with the major difficulty being that the non-equilibrium surface forces are time- (process-) dependent. A recent review on the non-equilibrium surface tension is available in works.[35,36]

We develop a novel approach that is based on the phase-field (Cahn-Hilliard) model.[23,24] The approach allows incorporation of the dynamic (non-equilibrium) capillary pressure into the hydrodynamic equations. Recently,[33,37,38] we found that the non-equilibrium surface tension influences the dynamics of miscible systems on a short (hydrodynamic) time scale (after the moment of the first contact of two miscible liquids), setting the shapes of interfaces (and setting the diffusion rates that are proportional to the area of contact). Diffusion controls the dynamics of miscible liquids on a longer (diffusive) time scale, smearing the interfaces and lowering the surface tension forces.

In this work we apply the new approach for investigation of the dynamics of a miscible displacement in a capillary. The major result of this research is the direct dynamic calculations of the non-equilibrium capillary pressure of a miscible interface in a capillary. We show that at the first contact of two miscible liquids, the capillary pressure rapidly drops to low but non-zero value. At the later moments, the changes of the capillary pressure happen much slower. In particular, when the liquids are miscible in all proportions, the capillary pressure of a meniscus drops with time with the law that is close to $t^{-0.5}$. The capillary pressure slows down the flow rate through a capillary. The time-dependence of the capillary

pressure makes the flow rate time-dependent as well.

The non-equilibrium capillary pressure of a miscible interface is a novel physical effect that can be experimentally verified using a rig similar to the one used in the experiment,[12] taking capillaries of smaller diameter and replacing optical observations by measurements of the flow rate. Understanding of this effect will improve control of the dynamics of miscible multiphase flows that take place in a number of technologies, when the porous matrix is initially saturated with one liquid, and when another liquid is injected into the porous matrix to displace (or wash out) the first liquid.

Acknowledgement

This research work is partially financially supported by the Russian Foundation for Basic Research (grant 18-01-00782) and by the Tomsk Polytechnic University CE Program. The authors acknowledge the use of the IRIDIS High Performance Computing Facility, and associated support services at the University of Southampton, in the completion of this work.

References

(1) Mukhopadhyay, M. *Natural extracts using supercritical carbon dioxide*; CRC Press LLC., 2000.

(2) Babadagli, T. Development of mature oil fields — A review. *J. Petroleum Sci. Eng.* **2007**, *57*, 221–246.

(3) Emami-Meybodi, H.; Hassanzadeh, H.; P.Green, C.; Ennis-King, J. Convective dissolution of CO2 in saline aquifers: Progress in modeling and experiments. *Int J Greenhouse Gas Control* **2015**, *40*, 238–266.

(4) Jawitz, J. W.; Annable, M. D.; Rao, P. S. C. Miscible fluid displacement stability in

unconfined porous media: Two-dimensional flow experiments and simulations. *J. of Contaminant Hydrology* **1998**, *31*, 211–230.

(5) Das, D. B., Hassanizadeh, S. M., Eds. *Upscaling Multiphase Flow in Porous Media*; Springer, 2005.

(6) Joseph, D. Fluid dynamics of two miscible liquids with diffusion and gradient stresses. *European Journal of Mechanics B/Fluids* **1990**, *9*, 565–596.

(7) Pojman, J. A.; Whitmore, C.; Liveri, M. L. T.; Lombardo, R.; Marszalek, J.; Parker, R.; Zoltowski, B. Evidence for the Existence of an Effective Interfacial Tension between Miscible Fluids: Isobutyric Acid-Water and 1-Butanol-Water in a Spinning-Drop Tensiometer. *Langmuir* **2006**, *22*, 2569–2577.

(8) Zoltowski, B.; Chekanov, Y.; Masere, J.; Pojman, J. A.; Volpert, V. Evidence for the Existence of an Effective Interfacial Tension between Miscible Fluids. 2. Dodecyl Acrylate-Poly(dodecyl acrylate) in a Spinning Drop Tensiometer. *Langmuir* **2007**, *23*, 5522–5531.

(9) Truzzolillo, D.; Mora, S.; Dupas, C.; Cipelletti, L. Nonequilibrium interfacial tesnsion in simple and complex fluids. *Physical Review X* **2016**, *6*, 041057.

(10) Gauthier, G.; Martin, J.; Salin, D. Gravity Waves at the Interface between Miscible Fluids and at the Top of a Settling Suspension. *Phys. Rev. Let.* **2005**, *94*, 204501.

(11) Shevtsova, V.; Gaponenko, Y.; Yasnou, V.; Mialdun, A.; Nepomnyashchy, A. Wall-Generated Pattern on a Periodically Excited Miscible Liquid/Liquid Interface. *Langmuir* **2015**, *31*, 5550–5553.

(12) Petitjeans, P.; Maxworthy, T. Miscible displacements in capillary tubes. Part 1. Experiments. *Journal of Fluid Mechanics* **1996**, *326*, 37–56.

(13) Chen, C.-Y.; Meiburg, E. Miscible displacements in capillary tubes. Part 2. Numerical simulations. *Journal of Fluid Mechanics* **1996**, *326*, 57–90.

(14) Legendre, M.; Petitjeans, P.; Kurowski, P. Instabilites a l'interface entre fluides miscibles par forcage oscillant horizontal. *C. R. Mecanique* **2003**, *331*, 617–622.

(15) Stevar, M.; Vorobev, A. Shapes and dynamics of miscible liquid/liquid interfaces in horizontal capillary tubes. *Journal of Colloid and Interface Science* **2012**, *383*, 184–197.

(16) Carbonaro, A.; Cipelletti, L.; Truzzolillo, D. Ultralow effective interfacial tension between miscible molecular fluids. *Phys. Rev. Fluids* **2020**, *5*, 074001.

(17) Freundlich, H. *Colloid and Capillary Chemistry*; Methuen & Co Ltd., 1926.

(18) Vorobev, A.; Boghi, A. Phase-field modelling of a miscible system in spinning droplet tensiometer. *Journal of Colloid and Interface science* **2016**, *482*, 193–204.

(19) Barenblatt, G. I.; Patzek, T. W.; Silin, D. B. The mathematical model of nonequilibrium effects in water-oil displacement. *SPE Journal* **2003**, 87329.

(20) Niessner, J.; Berg, S.; Hassanizadeh, S. M. Comparison of two-phase Darcy's law with a thermodynamically consistent approach. *Transport in porous media* **2011**, *88*, 133–148.

(21) Vorobev, A.; Prokopev, S.; Lyubimova, T. Phase-field modelling of a liquid/liquid immiscible displacement through a network of capillaries. *Journal of Computational Physics* **2020**, *421*, 109747.

(22) Lowengrub, J.; Truskinovsky, L. Quasi-incompressible Cahn-Hilliard fluids and topological transitions. *Proc. R. Soc. London, Ser. A* **1998**, *454*, 2617–2654.

(23) Vorobev, A. Boussinesq approximation of the Cahn-Hilliard-Navier-Stokes equations. *Phys. Rev. E* **2010**, *82*, 056312.

(24) Vorobev, A.; Lyubimova, T. Vibrational convection in a heterogeneous binary mixture. Part 1. Time-averaged equations. *J. Fluid Mech.* **2019**, *870*, 543–562.

(25) Landau, L. D.; Lifshitz, E. M. *Statistical Physics. Volume 5 of the Course of Theoretical Physics*; Elsevier, 1987.

(26) Jacqmin, D. Contact-line dynamics of a diffusive fluid interface. *Journal of Fluid Mechanics* **2000**, *402*, 57–88.

(27) Cahn, J. W.; Hilliard, J. E. Free Energy of a Nonuniform System. I. Interfacial Free Energy. *Journal of Chemical Physics* **1958**, *28*, 258–267.

(28) Ngan, C. G.; Dussan V., E. B. On the nature of the dynamic contact angle: an experimental study. *Journal of Fluid Mechanics* **1982**, *118*, 27–40.

(29) Ferziger, J. H.; Peric, M. *Computational Methods for Fluid Dynamics*; Springer, 2002.

(30) Guermond, J. L.; Minev, P.; Shen, J. An overview of projection methods for incompressible flows. *Computer methods in applied mechanics and engineering* **2006**, *195*, 44–47.

(31) Prokopev, S.; Vorobev, A.; Lyubimova, T. Phase-field modeling of an immiscible liquid-liquid displacement in a capillary. *Physical Review E* **2019**, *99*, 033113.

(32) Washburn, E. W. The dynamics of capillary flow. *Proc. R. Soc. A* **1921**, *17*, 273–283.

(33) Lyubimova, T.; Vorobev, A.; Prokopev, S. Rayleigh-Taylor instability of a miscible interface in a confined domain. *Phys. Fluids* **2019**, *31*, 014104.

(34) Korteweg, D. J. Sur la forme que prennent les equations du mouvement des fluides si l'on tient compte des forces capillaires causees par des variations de densite considerables mais continues et sur la theorie de la capillarite dans l'hypothese d'une variation continue de la densite. *Archives Neerlandaises des Sciences Exactes et Naturelles* **1901**, *6*, 1–24.

(35) Vorobev, A. Dissolution dynamics of miscible liquid/liquid interfaces. *Curr. Opin. Colloid Interface Sci.* **2014**, *19*, 300–308.

(36) Truzzolillo, D.; Cipelletti, L. Off-equilibrium surface tension in miscible fluids. *Soft Matter* **2017**, *13*, 13–21.

(37) Vorobev, A.; Khlebnikova, E. Modelling of the rise and absorption of a fluid inclusion. *Int. J. Heat Mass Trans.* **2018**, *125*, 801–814.

(38) Vorobev, A.; Zagvozkin, T.; Lyubimova, T. Shapes of a rising miscible droplet. *Physics of Fluids* **2020**, *32*, 012112.

Graphical TOC Entry